

Developmental Cell, Volume 60

Supplemental information

**RIF1 controls replication timing in early mouse
embryos independently of lamina-associated
nuclear organization**

Tsunetoshi Nakatani, Tamas Schauer, Mrinmoy Pal, Andreas Ettinger, Luis Altamirano-Pacheco, Julia Zorn, David M. Gilbert, and Maria-Elena Torres-Padilla

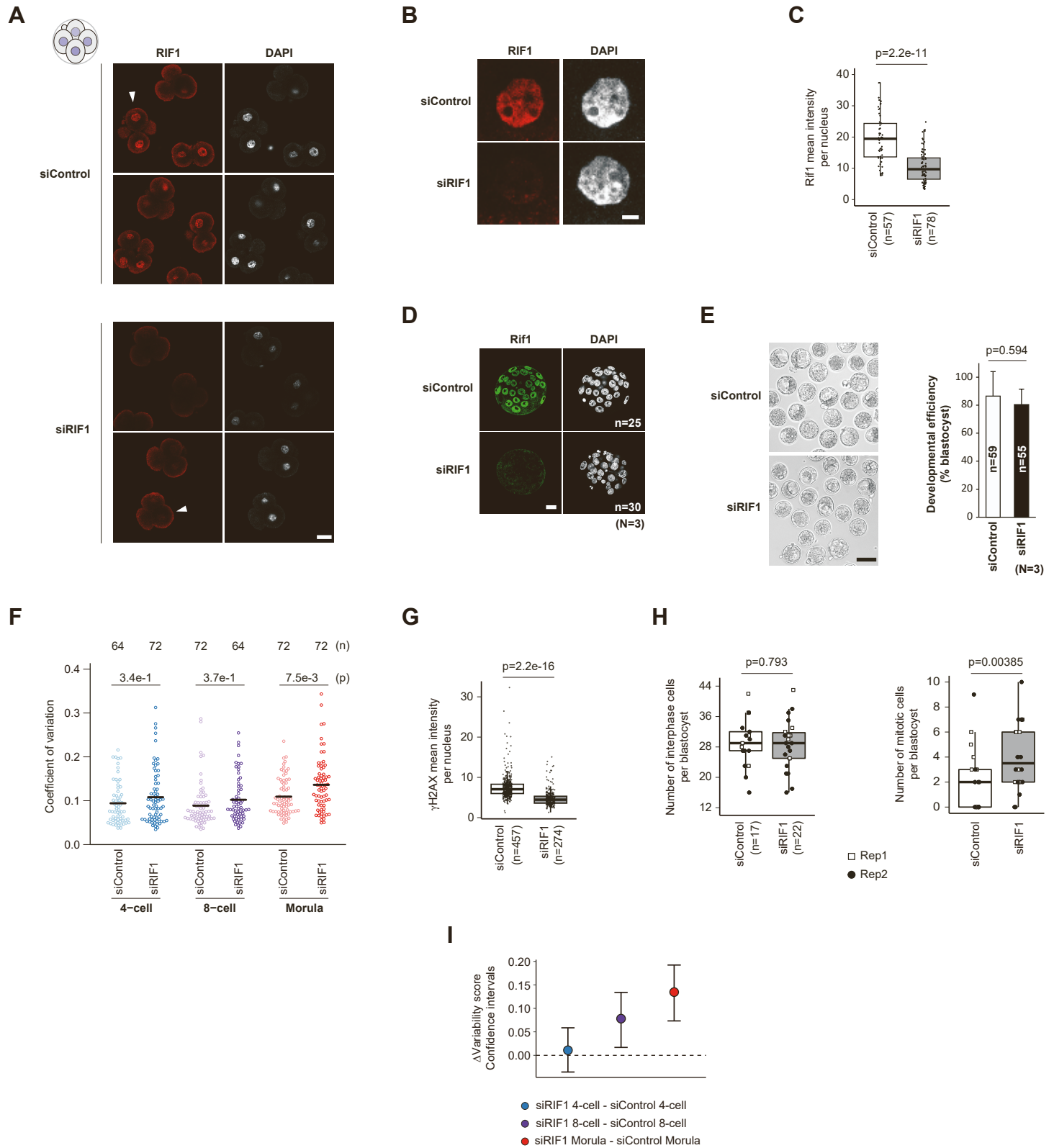


Figure S1, related to Figure 1. Developmental phenotype after RIF1 depletion.

(A) RIF1 immunostaining in several 4-cell stage control embryos and embryos microinjected with siRNA for RIF1 showing reproducible reduction in nuclear RIF1 protein. The embryo indicated with an arrowhead is the same embryo shown in Figure 1. Shown are single confocal sections. Scale bar, 25 μm .

(B) Representative nuclei of a 4-cell control or RIF1-depleted embryo following RIF1 immunostaining indicating depletion of RIF1 in the nucleus upon siRNA injection. Scale bar, 5 μm .

(C) Quantification of RIF1 levels in 4-cell stage control embryos and embryos microinjected with siRNA for RIF1 based on the mean intensity of fluorescence in each nucleus. Dots represent each nucleus (n).

(D) RIF1 immunostaining at the blastocyst stage after microinjection of control siRNA or siRNA for RIF1. Scale bar, 25 μm .

(E) Developmental progression of embryos upon RIF1 depletion. Zygotes collected at 17-18 h post-hCG were microinjected with siRNA for control or against *Rif1* and cultured until 96 h post-hCG. Representative image of a RIF1-depleted embryo (E) after immunostaining for RIF1. In (F), brightfield images of representative embryos (left) for both groups are shown. On the right, the percentage of embryos reaching the blastocyst stage is indicated; n: number of embryos analyzed from 3 (N) independent experiments. Statistical analyses are by two-sided Student's *t*-test. Mean \pm SD. Scale bar, 100 μm .

(F) Coefficient of variation calculated on the average read counts per chromosome using the scRepli-seq data. The number of cells analyzed in each stage are indicated on top (n). Black lines show mean. P-values were obtained by a linear model and were adjusted for multiple comparisons.

(G) Quantification of the signal intensity of γH2AX at morula stage upon RIF1 depletion. n: number of nuclei analyzed from two independent experiments. n: number of analyzed nuclei.

(H) Quantification of the number of interphase (left) and mitotic (right) cells per blastocyst in control embryos or after depletion of RIF1. White rectangles and black circles indicate the values of each replicate. P-values were calculated by a generalized linear model of the Poisson family. n: number of analyzed embryos. On the right panel, the mean values for replicate 1 are 1.45 mitotic cells per blastocyst in controls and 3.73 in siRIF1 embryos (median for siControl is 0 and for siRIF1 is 3 cells). For replicate 2, the mean number of mitotic cells per blastocyst is of 3.83 for control embryos and of 4.57 for siRIF1 embryos (median for siControl is 3.5 and for siRIF1 is 6 cells).

(I) Statistical analysis of data in Figure 1K. Shown are the pairwise differences in the mean variability score between the siControl and siRIF1 embryos at the same stage. Error bars indicate the 95% bootstrap confidence intervals (CIs). CIs are calculated at the 95% confidence level and thus a CI that does not overlap with '0' indicates significance at the 0.05 level.

In C, G and H, box plots show median values and the interquartile range (IQR), whiskers depict the smallest and largest values within $1.5 \times \text{IQR}$.

Figure. S2, Nakatani, *et al.*

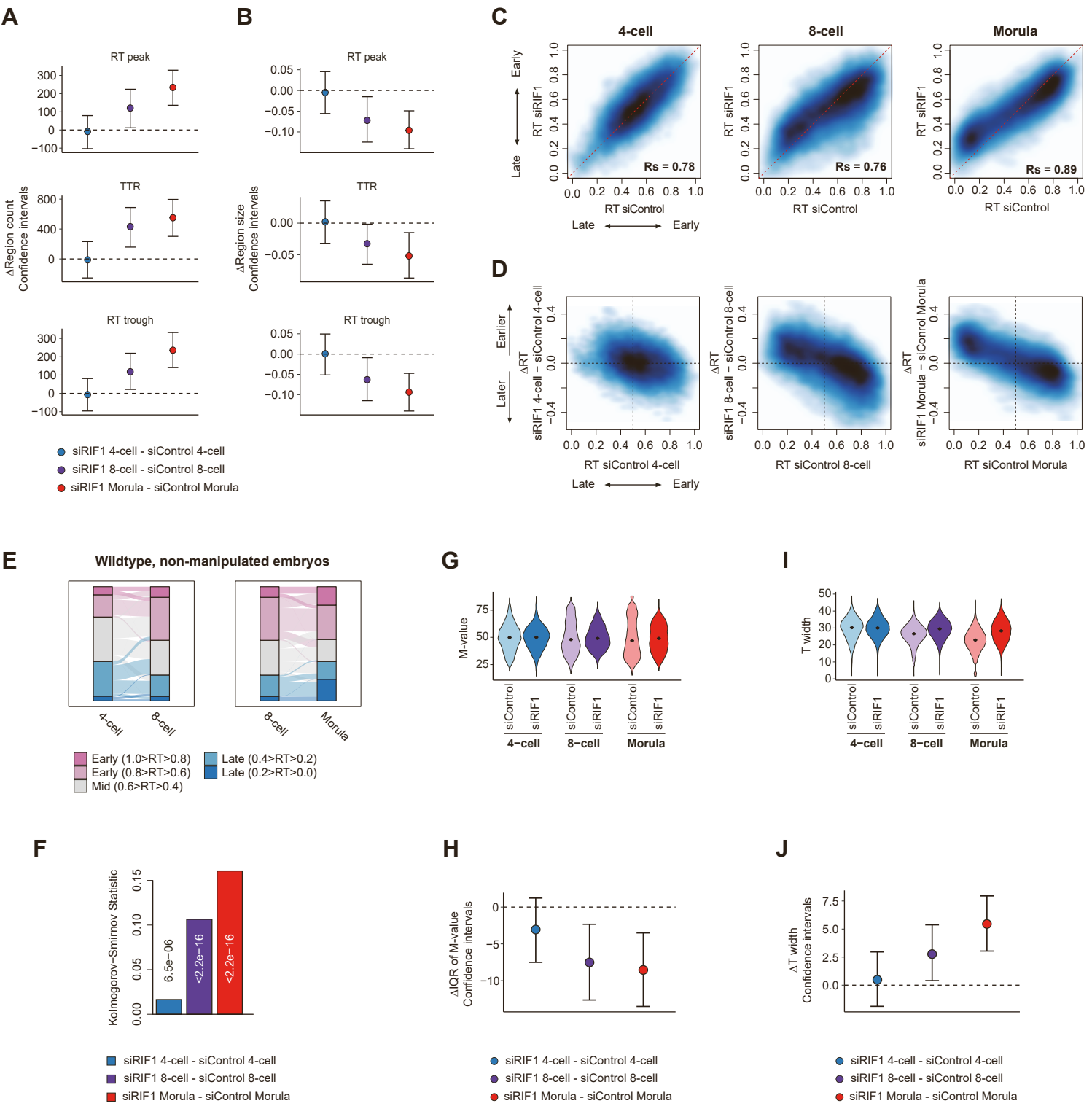


Figure S2, related to Figure 2. Depletion of RIF1 increases cell-to-cell heterogeneity of the RT program.

(A-B) Analysis of statistical significance of data in Figure 2A for the number (A) and size (B) of RT peaks, TTRs and RT troughs. Pairwise differences in the mean of the RT features in each developmental stage are plotted with error bars indicating the 95% bootstrap confidence intervals (CIs). CIs are calculated at the 95% confidence level and thus a CI that does not overlap with '0' indicates significance at the 0.05 level.

(C) Smoothed scatter plots of RT values in control (siControl) compared to RIF1-depleted embryos (siRIF1). Rs: Spearman's correlation.

(D) Smoothed scatter plots comparing the RT values in control (siControl) versus the differences in RT (Δ RT) between RIF1-depleted and control embryos at the indicated stages.

(E) Alluvial plot depicting RT changes of all genomic bins showing changes of RT in wild-type, unperturbed embryos (GSE218365) as development proceeds. RT values were categorised in 5 groups from the earliest ($1.0 > RT > 0.8$) to latest RT ($0.2 > RT > 0.0$) across the genome.

(F) Statistical analysis of Figure 2E. Bar plot showing the Kolmogorov-Smirnov statistic and the corresponding p-values indicating whether two samples (siRIF1 vs. siControl) came from the same distribution.

(G) Violin plots showing the M -value, which is the replication score at which 50% of the cells replicated a given 50kb bin of the indicated experimental and control groups.

(H) Statistical analysis of S2G. Pairwise differences in the interquartile range (IQR) of M -values in each developmental stage are plotted with error bars indicating the 95% bootstrap confidence intervals.

(I) Violin plot depicting the T_{width} , which is the replication score difference between 25% and 75% of cells replicated the 50kb bin, at the indicated experimental and control groups.

(J) Statistical analysis of S2I. Pairwise differences in the mean of T_{width} in each developmental stage are plotted with error bars indicating the 95% bootstrap confidence intervals.

In G and I, each violin shows the distribution of scores for all genomic bins and dots indicate median.

Figure. S3, Nakatani, *et al.*

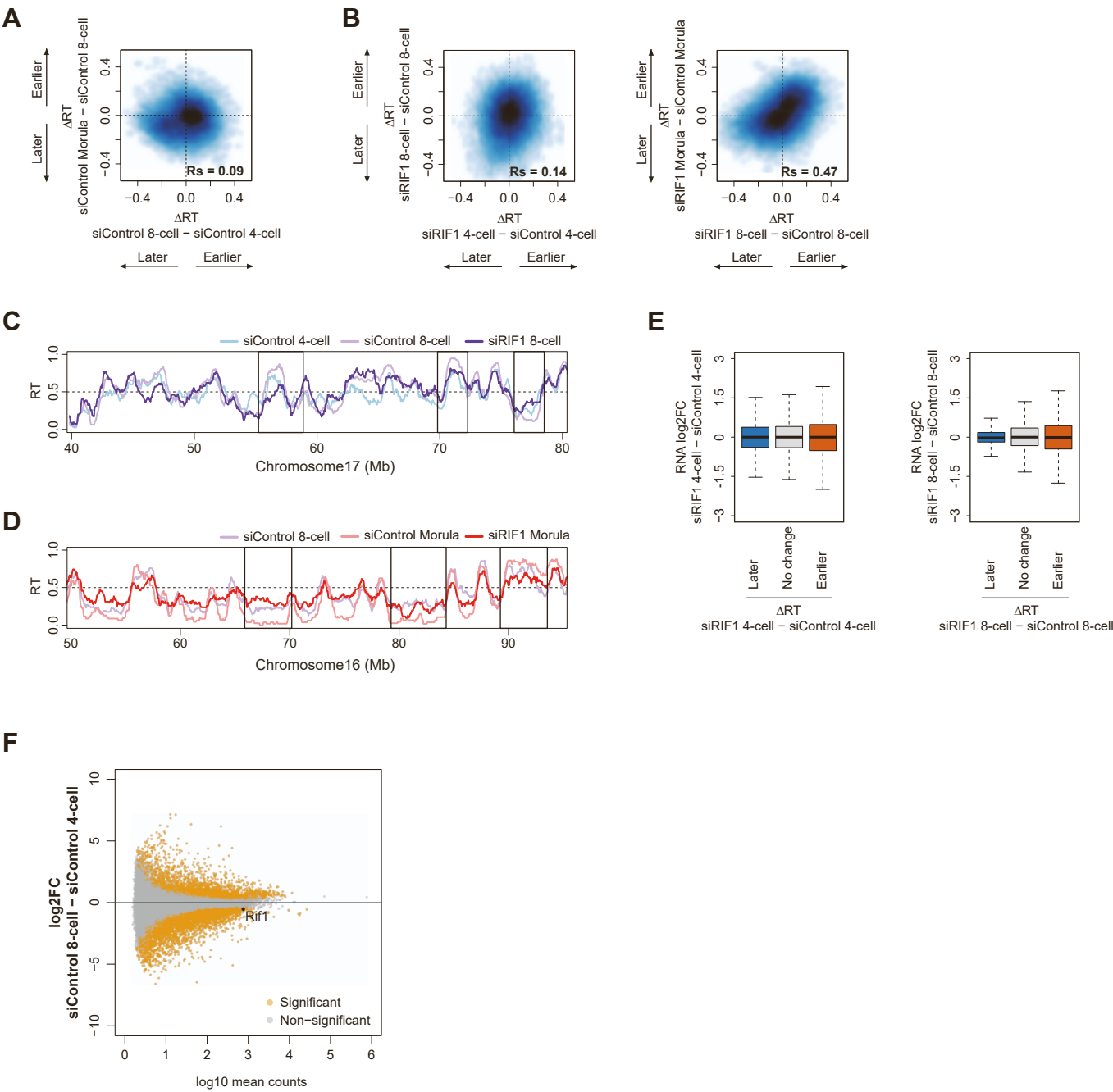


Figure S3, related to Figure 3. RIF1 regulates replication timing in a stage-specific manner.

(A) Smoothed scatterplot of RT differences (Δ RT) between morula and 8-cell stage of control siRNA injected embryos versus RT differences (Δ RT) between 8-cell and 4-cell stage of control siRNA injected embryos.

(B) Smoothed scatterplot of RT differences (Δ RT) between same stages of RIF1-depleted (siRIF1) and control (siControl) embryos versus RT differences (Δ RT) between same stages of RIF1-depleted and control injected embryos.

(C and D) Representative RT profiles where regions that change RT during development display an opposite direction in RT change due to RIF1 depletion. 4- to 8-cell stage (C), and 8-cell stage to morula (D) patterns are shown.

(E) Changes in RNA expression (\log_2 FC) between RIF1-depleted (siRIF1) and control (siControl) embryos across genomic bins displaying differential RT changes upon RIF1 depletion in 4-cell and 8-cell stage embryos. Box plots show median and the interquartile range (IQR), whiskers depict the smallest and largest values within $1.5 \times \text{IQR}$.

(F) MA plot showing differentially expressed genes between control (siControl) embryos at the 8-cell stage compared to control 4-cell stage embryos. P-values were obtained by DESeq2.

In A and B, Rs: Spearman's correlation.

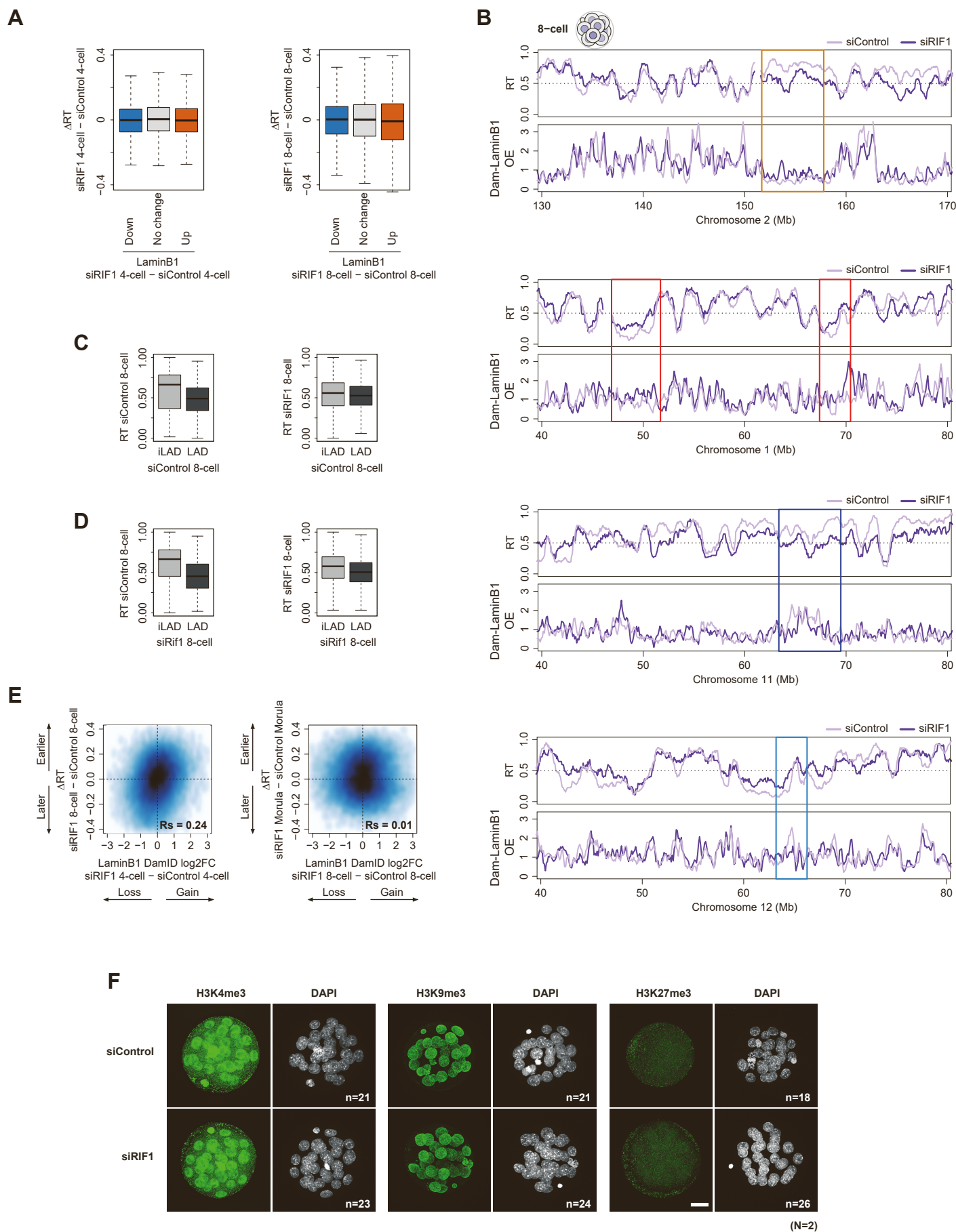


Figure S4, related to Figure 4. Changes of RT and remodelling of LADs distribution are independent upon RIF1 depletion.

(A) Box plots depicting differences in RT (ΔRT) between RIF1-depleted (siRIF1) and control (siControl) embryos at genomic bins with significantly increased (red) and decreased (blue) lamina interactions upon RIF1 depletion at indicated stages. Box plots show median and the interquartile range (IQR), whiskers depict the smallest and largest values within $1.5 \times IQR$.

(B) Representative examples of changes in RT and genome-lamina interactions upon RIF1 depletion at the 8-cell stage. For each track example, regions marked by the colored rectangles show different types of behavior. The color code corresponds to the colors in Figure 4D: later replication and gained lamina interaction upon RIF1 depletion (top, yellow); earlier replication and gained lamina interaction upon RIF1 depletion (second row, red); later replication and reduced lamina interaction upon RIF1 loss (third row, darker blue), and earlier replication with reduced lamina interaction upon RIF1 depletion (bottom, lighter blue).

(C and D) Box plots depicting RT values of RIF1-depleted (siRIF1) and control (siControl) 8-cell embryos in iLADs and LADs from control (B) and from RIF1-depleted (C) embryos.

(E) Smoothed scatter plots of RT differences (ΔRT) between same stages of RIF1-depleted (siRIF1) and control (siControl) embryos versus changes in Dam-LaminB1 OE values ($\log_2 FC$) at the earlier developmental stage as indicated. Rs: Spearman's correlation.

(F) Immunostaining of histone H3 lysine 4 trimethylation (H3K4me3), histone H3 lysine 9 trimethylation (H3K9me3), and histone H3 lysine 27 trimethylation (H3K27me3) in morula stage embryos after depletion of RIF1. Representative maximum intensity projection images are shown. Total number of embryos (n) analyzed in each condition from two independent experiments (N) are shown. Scale bar, 25 μm .